


Absence of Partial Amorphization in GeSbTe Chalcogenide Superlattices

Valentin Evang and Riccardo Mazzarello*

Phase-change materials (PCMs) are widely used for optical data storage due to their fast and reversible transitions between a crystalline and an amorphous phase that exhibit reflectivity contrast. In the last decade, PCMs have been found to be promising candidates for the development of nonvolatile electronic memories, as well. In this context, superlattices of thin layers of GeTe and Sb₂Te₃ show an unprecedented performance gain in terms of switching speed and power consumption with respect to bulk GeSbTe compounds. Models of crystalline–crystalline transitions, proposed to explain the improved properties, however, are challenged by recent experiments in which GeTe–Sb₂Te₃ superlattices are observed to reconfigure toward a van der Waals heterostructure of rhombohedral GeSbTe and Sb₂Te₃. Herein, *ab initio* molecular dynamics simulations are used to explore an alternative switching mechanism that comprises amorphous–crystalline transitions of ultrathin GeSbTe layers between crystalline Sb₂Te₃. Despite some positive results obtained by tailoring the quenching protocol, overall the extensive simulations do not yield clear evidence for this mechanism. Therefore, they suggest that the switching process probably involves a transition between two crystalline states.

Phase-change materials (PCMs) can be switched fast and reversibly between an amorphous (RESET) and a crystalline state (SET),^[1] which show a pronounced difference in reflectivity and resistivity. These properties and the high stability of both phases at room temperature, as well as the good spatial scalability, enable these materials to be used not only for optical data storage,^[2] where the transitions are triggered by laser pulses, but also for nonvolatile electronic memory,^[3,4] which is set and reset by voltage pulses. PCMs are already used in storage class memory devices.^[5] Two key issues affecting the prospects for PCMs to replace dynamic random-access memory or FLASH technology are, respectively, the switching speed and the power consumption.

V. Evang, Prof. R. Mazzarello
 Institute for Theoretical Solid-State Physics, JARA-FIT and JARA-HPC
 RWTH Aachen University
 Aachen 52056, Germany
 E-mail: mazzarello@physik.rwth-aachen.de

 The ORCID identification number(s) for the author(s) of this article can be found under <https://doi.org/10.1002/pssr.202000457>.

© 2020 The Authors. Published by Wiley-VCH GmbH. This is an open access article under the terms of the Creative Commons Attribution-NonCommercial-NoDerivs License, which permits use and distribution in any medium, provided the original work is properly cited, the use is non-commercial and no modifications or adaptations are made.

DOI: 10.1002/pssr.202000457

GeTe and Sb₂Te₃, the parent compounds of the important class of GeSbTe (GST) PCMs, were shown by Chong et al.^[6] to exhibit fairly improved switching properties with respect to the bulk GST alloy if they are deposited alternatively in a superlattice-like fashion with layer thicknesses of several nanometers. The improved efficiency of these superlattices was attributed to enhanced thermal confinement. Subsequently, Simpson et al.^[7] obtained a much more significant gain in switching speed, energy efficiency, and cyclability with superlattices of reportedly only 1 nm thick layers of GeTe and Sb₂Te₃. The authors concluded that the present system, dubbed interfacial phase-change memory (IPCM), performs crystalline–crystalline transitions via dimensionally constrained motion of Ge atoms at the GeTe–Sb₂Te₃ interface, thus avoiding the energy-demanding bulk melting and involving low entropic losses. Subsequently, two competing switching models^[8–13] were proposed, both of which comprise Ge atoms hopping into the so-called van der Waals (vdW) gaps between two adjacent, weakly bonded Te layers.

Molecular beam epitaxy (MBE) experiments by Momand et al.,^[14] however, challenge the picture of a superlattice of nanometer thick sublayers of (GeTe)₂ and Sb₂Te₃ and thus also call into question the proposed switching models. The authors report that despite the high accuracy of the method used by them to form such superlattice, the material reconfigures already during growth into a heterostructure of Sb₂Te₃ on the one hand and layers of stable, rhombohedral GST (Kooi-like^[15] structures) on the other hand, with vdW gaps separating the two building blocks. Furthermore, pronounced stacking disorder and the formation of different GST layers with varying stoichiometry are reported. For example, seven-layer and nine-layer blocks of the sequence Te–Sb–Te–Ge–Te–Sb–Te (respectively, Te–Sb–Te–Ge–Te–Ge–Te–Sb–Te) with some degree of compositional Ge/Sb disorder are found. Similar results are obtained by growing the superlattices by pulsed laser deposition.^[16] These blocks also occur in the stable bulk phase of the corresponding GST stoichiometry. In summary, it is shown that intercalating GeTe into Sb₂Te₃ quintuple layers (QLs) is thermodynamically preferred, ruling out switching models that rely on a separation of these two compounds and on Ge atoms lying close to vdW gaps. Recently, new models for the switching mechanism have been proposed on the basis of these findings.^[17–20] In these models, the switching is associated with a reconfiguration of the vdW gaps through the inversion of

Sb–Te (or Ge/Sb–Te) bilayers between neighboring blocks. These bilayer defects are frequently observed in sputter-deposited, annealed GST and Sb_2Te_3 and are stabilized by Sb–Te intermixing.^[21,22]

In the study by Momand et al.,^[14] on the other hand, it is suggested that the switching in the superlattices may be “a limiting case of the amorphous–crystalline transition of very thin GST sublayers sandwiched between Sb_2Te_3 Qs.” Regarding the RESET transition, it is conjectured that tensile strain in the GST layers caused by the Sb_2Te_3 Qs reduces the amorphization energy of the former. Furthermore, the crystallization of GST and thus the SET process could be accelerated by the presence of the crystalline Sb_2Te_3 matrix and evolve via template growth. This is supported in a very recent work^[23] in which superlattices of rock-salt-like Sb_2Te_3 and amorphous GST layers have been fabricated by atomic deposition and proper thermal annealing. Crystallization of GST is indeed shown therein to be accelerated by the presence of the Sb_2Te_3 template. Together, these effects could explain the improved performance with respect to bulk GST. In addition, other recent measurements^[24,25] give a reduced thermal conductivity in IPCMs with respect to bulk GST, similarly to the behavior of the superlattices with thicker blocks,^[6] which speaks in favor of the explanation of reduced switching energy via thermal confinement.

The experimental results and the conjectures of the study by Momand et al.^[14] call for a theoretical approach to explore switching processes based on partial amorphization in these vdW heterostructures. The central question addressed here is whether, by ultrafast heating and quenching, it is possible to amorphize the rhombohedral GST sublayers while keeping the Sb_2Te_3 Qs crystalline and preserving the overall vdW structure. We thus use ab initio molecular dynamics (AIMD) for assessing the behavior of such a heterostructure.

The superlattice model examined in this article uses periodic boundary conditions and consists of an Sb_2Te_3 QL and a 7-layer $\text{Ge}_1\text{Sb}_2\text{Te}_4$ block making up a total of 12 atomic layers in the primitive cell, yielding an ABC stacking of the atomic layers

without stacking or twinning faults. The model is shown in **Figure 1a**. The choice of this model is dictated by computational convenience. The resulting sequence ...–Te–Sb–Te–Te–Sb–Te–Ge–Te–Sb–Te–Te–Sb–... corresponds to the stable phase of $\text{Ge}_1\text{Sb}_2\text{Te}_4$ ^[26] comprising two vdW gaps (Te–Te) per cell. The supercell is chosen to be orthorhombic with the z-axis perpendicular to the atomic planes, and it contains 360 atoms in total with 30 atoms per layer. A preliminary NPT simulation at room temperature results in an atomic density of $n = 0.03114 \text{ \AA}^{-3}$ and an in-plane lattice constant of $a = 4.30 \text{ \AA}$. From an analogous NPT simulation of pure $\text{Ge}_1\text{Sb}_2\text{Te}_4$, which yields a theoretical lattice constant of 4.28 \AA , we find that in the superlattice, the septuple layer is subjected to a relative tensile strain of about 0.5%.

The system is heated to $\approx 1500 \text{ K}$, i.e., around 600 K above the experimental bulk melting points of the constituting materials, to enhance structural fluctuations and thus accelerate the creation of a melting seed. Without such overheating, it would not be possible to observe melting on the timescales accessible by AIMD simulations. This is a drawback of the simulations, which can in principle promote the rapid melting of both blocks and, thus, hinder partial melting. The first 110 ps are characterized by premelt disordering events in the overheated crystal, which are much more pronounced in $\text{Ge}_1\text{Sb}_2\text{Te}_4$ than in Sb_2Te_3 : When screening the trajectory for atoms that leave their crystalline positions beyond the high-temperature oscillations, it turns out that such events affect 23% of the atoms belonging to $\text{Ge}_1\text{Sb}_2\text{Te}_4$ but only 4% of the Sb_2Te_3 atoms. The fraction is especially high for Ge atoms (37%), as reflected by the mean square displacements shown in **Figure 2a**.

After 110 ps, a region of pronounced disorder starts to grow inside the $\text{Ge}_1\text{Sb}_2\text{Te}_4$ block near the upper vdW gap. Not surprisingly, melting affects the whole supercell within a couple of picoseconds at a temperature of 1500 K. Since the high temperature is only needed to *trigger* the melting process, it is in the following gradually lowered. To this end, the trajectory is monitored: Once the molten region inside the $\text{Ge}_1\text{Sb}_2\text{Te}_4$ block grows critically

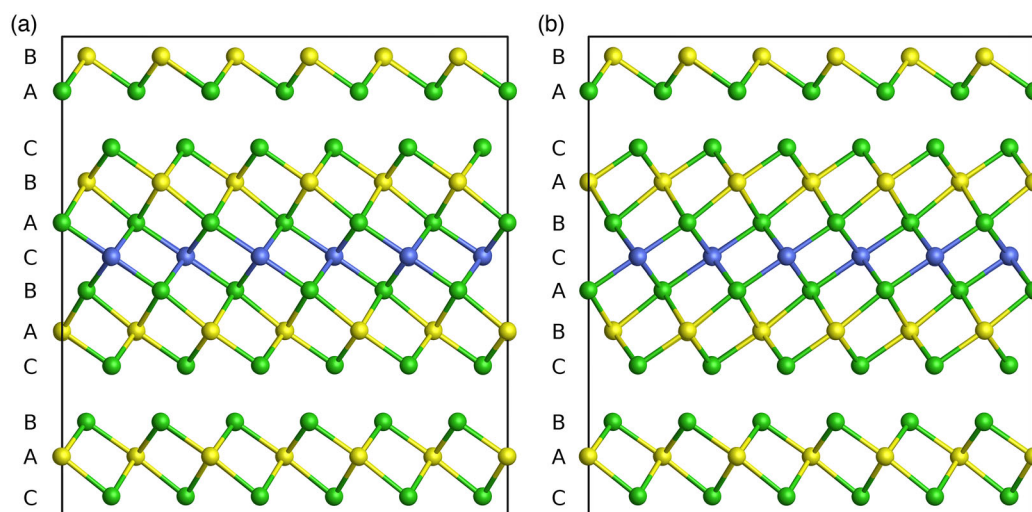


Figure 1. a,b) Crystalline 360-atom models of the superlattices without (a) and with (b) twinning. The periodic supercells contain Ge (blue), Sb (yellow), and Te atoms (green) in alternating sequences of rhombohedral $\text{Ge}_1\text{Sb}_2\text{Te}_4$ and Sb_2Te_3 . The model with twinning comprises changes in the ABCBC stacking direction at the vdW gaps.

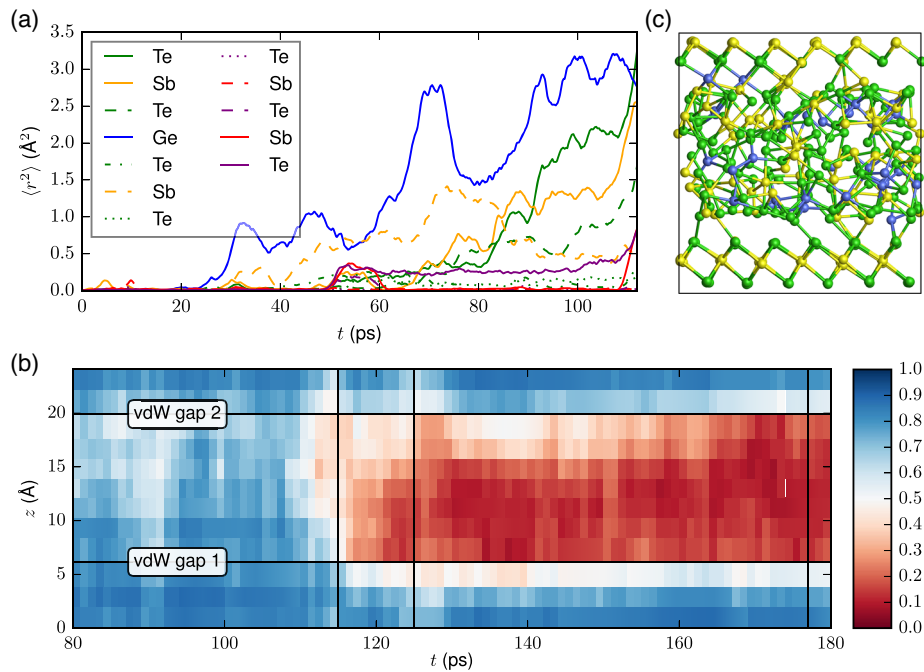


Figure 2. a) Mean square displacements of the atoms showing the pronounced premelt disorder in the $\text{Ge}_1\text{Sb}_2\text{Te}_4$ layer during the first phase of the simulation. Each of the 12 curves represents the average over the 30 atoms initially belonging to the same atomic layer in the perfectly crystalline superlattice. The order of the legend entries reflects the sequence of atomic layers, and the left column in the legend corresponds to the $\text{Ge}_1\text{Sb}_2\text{Te}_4$ layer. For a better visual impression, the trajectory has been smoothed with a 3 ps sliding window before calculating the displacements. b) Evolution of the layer-averaged q_4^{dot} showing the melting process of the superlattice. The blue color corresponds to the crystalline phase, whereas the red bins correspond to molten regions. Vertical lines mark the three abrupt quenches in the target temperature of the thermostat that are necessary to guide the model into a partially liquid ($\text{Ge}_1\text{Sb}_2\text{Te}_4$), partially crystalline (Sb_2Te_3) state. The bins along the z -axis are chosen to best capture the individual atomic planes of the initially crystalline superlattice. c) Final state of the partly amorphous, partly crystalline superlattice quenched to 0 K.

and starts to affect the rest of the system, the simulation is split into several branches with various lower thermostat temperatures. In addition to higher- T branches that lead to a complete melt and lower- T branches where the system recrystallizes, there are thermostat settings that keep the region inside the $\text{Ge}_1\text{Sb}_2\text{Te}_4$ block liquid while preventing the disorder from expanding over the whole supercell. At the start of a new branch, the target temperature is lowered abruptly (leading to high but finite effective quenching rates since it takes time for the system to reach the new target temperature). This procedure is repeated several times. After three quenches, which are performed at 115, 125, and 177 ps, respectively, and lead to a maximum effective quenching rate of 25 K ps^{-1} , the system has cooled below 900 K and transitioned into a partially liquid ($\text{Ge}_1\text{Sb}_2\text{Te}_4$), partially crystalline (Sb_2Te_3) state. Figure 2b shows the layer-wise evolution of an order parameter discriminating between crystalline-like and liquid-like or amorphous-like atoms. A subsequent simulation at around 825 K assures that the system can maintain this phase over a period of at least 200 ps. The evaluation of atomic mean square displacements in the two different regions of the cell during this time span gives an estimate for the diffusion coefficient in the $\text{Ge}_1\text{Sb}_2\text{Te}_4$ region of $3 \times 10^{-10} \text{ m}^2 \text{ s}^{-1}$, whereas the solid Sb_2Te_3 QL only shows a small number of hopping events.

By quenching down the partially liquid system at a rate of 20 K ps^{-1} , one obtains a model containing amorphous $\text{Ge}_1\text{Sb}_2\text{Te}_4$ and crystalline Sb_2Te_3 as shown in Figure 2c.

To improve the statistics, ten more quenches starting from the partially liquid model at different frames are performed, each leading to a different, partially amorphous system.

On the basis of the partial pair-correlation functions of the amorphous material (see Figure S1, Supporting Information), which are computed with a scheme that takes into account the finite thickness of the relevant region in z -direction, the cutoffs necessary for bond-geometry analyses are defined. As an example for the structural properties of amorphous GST, the coexistence of octahedrally and tetrahedrally bonded Ge atoms^[27–31] is checked via the bond-order parameter $q = 1 - (3/8) \sum [1/3 + \cos(\theta_{ijk})]^2$,^[32] which gives 0.625 for an undistorted, fourfold octahedral environment and 1.0 for a perfectly tetrahedral coordination. The distribution of this parameter is shown in Figure S2, Supporting Information. With $q = 0.8$ as a threshold, 17% of all Ge atoms are found to be bonded tetrahedrally, comparing to 33% in bulk amorphous $\text{Ge}_2\text{Sb}_2\text{Te}_5$.^[27] The correlation between tetrahedral motifs and homopolar bonds (Ge–Ge and Ge–Sb) is clearly observed, as well: the fraction of Ge atoms with at least one homopolar bond rises from 35% to 67% if only tetrahedral Ge is considered; the stabilizing role of homopolar bonds for tetrahedral (sp^3) bonding^[27,30,31] is thus confirmed in our models.

Having found evidence for the partial amorphization of thin rhombohedral $\text{Ge}_1\text{Sb}_2\text{Te}_4$ between Sb_2Te_3 —at least for manual, adaptive quenching—it remains to be investigated how crystallization at elevated temperatures proceeds. The system is heated to

≈ 600 K, analogously to the study by Ronneberger et al.^[33] who simulate the crystallization of amorphous $\text{Ge}_2\text{Sb}_2\text{Te}_5$ from a crystalline matrix and obtain growth velocities on the order of $v_g = 1 \text{ m s}^{-1}$ at this temperature.

The local “dot-product” parameter q_4^{dot} ^[33,34] is used to distinguish crystalline from amorphous-like atoms, see the Computational Details section. **Figure 3** shows the trajectory on the basis of five screenshots chosen to represent the principal stages of the process. The main crystallization event commences at ≈ 150 ps and then proceeds extremely fast within another 150 ps. The most conspicuous feature is a “bridge”, see frame 175 ps, that spontaneously forms and connects the top of the $\text{Ge}_1\text{Sb}_2\text{Te}_4$ layer with a small region of ordered crystalline motifs in the lower half of the $\text{Ge}_1\text{Sb}_2\text{Te}_4$ layer. This region can be identified in the background in frame 150 ps. Further crystallization manifests itself as a widening of the bridge, which proceeds until only few noncrystalline atoms remain (frame 300 ps).

The final structure reflects an aspect that is already present in the initial, partly amorphous configuration, namely, a high concentration of Ge and Sb at the upper $\text{Ge}_1\text{Sb}_2\text{Te}_4$ – Sb_2Te_3 interface. The lower interface, on the other hand, comprises mostly Te atoms and therefore better resembles a vdW gap with weakly bonded Te layers. Interestingly, the observation that the major crystallization seed starts to expand from the top of the GST layer can be connected to the fact that the bonding of Ge and Sb atoms to the outermost Te layer of Sb_2Te_3 (which resembles the rock salt-like stacking of GST) has destroyed the vdW character of the upper interface. These additional bonds make the boundary chemically more active and accelerate crystallization. This is in line with the study by Feng et al.^[23], where it was shown that Sb_2Te_3 layers can act as templates and accelerate the crystallization of GST into a rock salt-like phase.

The initial success of bringing the superlattice into a partially amorphous state via trajectory monitoring and adaptive quenching needs to be subjected to critical testing. As a first check that is related to the cyclability of IPCMs, the recrystallized superlattice is heated again to simulate a second switching cycle. Due to the considerable structural disorder in the overall crystalline model, a temperature of about 1100 K is enough to trigger a melting event inside the $\text{Ge}_1\text{Sb}_2\text{Te}_4$ block after only 15 ps. By branching and quenching the system three times analogously to the first cycle, the system is again successfully guided into a partially liquid ($\text{Ge}_1\text{Sb}_2\text{Te}_4$), partially crystalline (Sb_2Te_3) state, which is confirmed to stably evolve at about 850 K over at least 140 ps. After a smooth quench to room temperature, the partially amorphous system recrystallizes at 580 K into a well-ordered

crystalline state within about 500 ps. The second switching cycle is shown in Figure S3 and S4, Supporting Information. The simulations show that initial structural disorder in the $\text{Ge}_1\text{Sb}_2\text{Te}_4$ block enhances the chances of partial melting, as the energetic barrier to overcome is considerably lowered and, from a technical point of view, more modest temperatures are sufficient to trigger the relevant events in a feasible time.

However, a second, independent attempt to partially amorphize the superlattice, starting from the perfect crystal, is less promising: Although melting starts again within the $\text{Ge}_1\text{Sb}_2\text{Te}_4$ block, no adaptive quenching procedure is able to melt this block while leaving Sb_2Te_3 intact. That even the manual branching method yields no positive result challenges the possibility of reproducible partial melting of the heterostructure. Moreover, although two switching cycles have been successfully performed on the superlattice, it is yet unclear if this would have been possible without active monitoring and adaptive quenching.

To answer this question, there is need for a systematic study that entails no manual intervention and allows to estimate the chances of partial amorphization from unbiased molecular dynamics runs. For this purpose, a very large set of simulations is conducted, each representing a side branch that starts from the original superlattice simulation during the premelting phase and undergoes a ramped quench. The onset time of the quench is varied in steps of 5 ps between the 70 ps and the 100 ps frame, and five quenching rates between 1 K ps^{-1} and 5 K ps^{-1} are used for each onset.

Figure 4a schematically shows the final states of the various simulations, which either end up completely crystalline or completely liquid. Although the $\text{Ge}_1\text{Sb}_2\text{Te}_4$ block is more strongly characterized by disorder than the Sb_2Te_3 QL in virtually all runs, and although almost all melting processes originate from somewhere in $\text{Ge}_1\text{Sb}_2\text{Te}_4$ (an exception being the trajectory in Figure 4b-iii), a stable separation into a liquid and a solid layer is observed in none of the 35 quenches. For each quenching rate and for each onset time (except for the branch starting at 75 ps), one finds simulations with either of the two possible outcomes, with a trend promoting melting for smaller quenching rates and later onset times. The fragility of the desired, partially liquid state cannot be practically overcome without further tuning the onset and quench rate, which, however, would again clearly bias the search toward a “successful” trajectory.

Whereas the superlattice considered here comprises vdW gaps that preserve the energetically preferred ABC stacking across the Te–Te layer boundary, stacking faults and twinning can frequently occur in heterostructures according to the study by

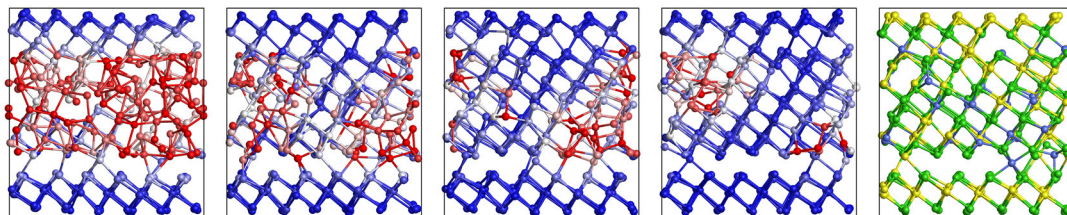


Figure 3. Screenshots of the superlattice during recrystallization. The figure shows, from left to right, the state of the model at 150, 175, 200, 275, and 300 ps after starting the high-temperature simulation (about 600 K). In the first four screenshots, atoms are colored according to their values of q_4^{dot} (blue: crystalline-like and red: amorphous-like).

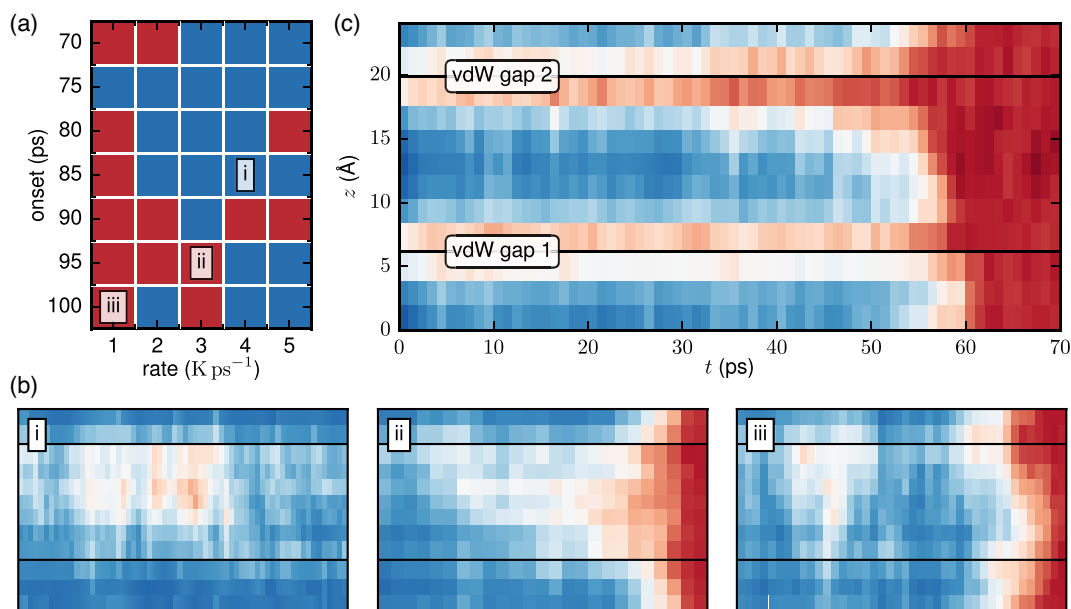


Figure 4. a) “Destiny map” depicting the final state (blue: crystalline and red: liquid) of each of the 35 unbiased quenches. b) Exemplary evolutions of q_4^{dot} from the unbiased simulations. The simulations include, e.g., i) temporary disorder in $\text{Ge}_1\text{Sb}_2\text{Te}_4$, ii) melting that starts from inside $\text{Ge}_1\text{Sb}_2\text{Te}_4$, and iii) melting that starts from regions around the vdW gaps. c) Evolution of the layer-averaged q_4^{dot} showing the melting process of the first of two superlattice models containing twinning at the vdW gaps. The same color bar as in Figure 2b applies.

Momand et al.^[14] Both features involve a deviation from the continuous ABCABC sequence of atomic planes. Applied to vdW gaps, we use the term “stacking fault” for a sequence that skips an atomic position, i.e., ABCBCA, corresponding to a layer of vacancies on an A site between neighboring Te layers. In contrast, “twinning” expresses itself as a change of stacking direction, i.e., ABCBA, where one of the Te layers is associated with the C site.

To examine the influence of a “non-ABC” vdW gap, we perform additional simulations of the supercell, but with the stacking direction of the $\text{Ge}_1\text{Sb}_2\text{Te}_4$ layer reversed. In this way, both vdW gaps exhibit twinning with changes of stacking direction occurring in the outer Te planes of $\text{Ge}_1\text{Sb}_2\text{Te}_4$. The model is shown in Figure 1b. Stacking faults cannot be inserted in our models because they require three or more gaps.

The evolution of disorder in one of two 1500 K runs is shown in Figure 4c (the second run is shown in Figure S5, Supporting Information). It is evident that the absence of octahedral coordination around the outer Te atoms leads to relatively low order around the vdW gaps from the very beginning. It is observed in both runs that the critical melting seed originates from one of the gaps and grows into both $\text{Ge}_1\text{Sb}_2\text{Te}_4$ and Sb_2Te_3 , even if an adaptive quenching procedure is used. At least in the second run, the GST block is affected earlier than the QL; however, any attempt to promote partial amorphization via the branching procedure fails as Sb_2Te_3 does not withstand the established disorder at its boundary. These observations strongly suggest that the frequent phenomenon of layering disorder destabilizes atomic layers on both sides of the vdW gaps at high temperatures and, hence, further prevents partial amorphization.

In summary, we have performed AIMD simulations of a $\text{Ge}_1\text{Sb}_2\text{Te}_4$ – Sb_2Te_3 heterostructure to examine its melting

behavior under high temperatures. In particular, the aim has been to assess the chances of partial amorphization of the thin GST sublayers as proposed in the study by Momand et al.^[14] to be the relevant mechanism in the fast and efficient switching processes observed in IPCMs in the study by Simpson et al.^[7]

In a first successful attempt, it has been possible to guide a 12-layer superlattice from a fully crystalline phase into a metastable, partially liquid ($\text{Ge}_1\text{Sb}_2\text{Te}_4$), partially crystalline (Sb_2Te_3) state following an adaptive quenching procedure. In this and all following simulations, we have found strong evidence that the $\text{Ge}_1\text{Sb}_2\text{Te}_4$ layer is more prone to melting than the QL. By analyzing the trajectories and mean square displacements, we have shown that this process is triggered by the high mobility of Ge atoms.

Although the adaptive quenching procedure allowed even a second cycle comprising partial melting, amorphization, and recrystallization, further quenches have shown that the manual intervention in the adaptive quenches was the decisive factor in establishing the fragile equilibrium of a nanometer-thick, crystalline Sb_2Te_3 QL and a liquid $\text{Ge}_1\text{Sb}_2\text{Te}_4$ layer. It is true that a liquid–solid coexistence, once obtained in a biased procedure, was maintained for several hundreds of picoseconds; however, no evidence was found that a single QL of Sb_2Te_3 can remain solid upon an onset of melting in the adjacent $\text{Ge}_1\text{Sb}_2\text{Te}_4$ layers in unbiased simulations. Furthermore, we have found that the presence of layering disorder at the vdW gaps [which is frequently observed in scanning transmission electron microscopy (STEM) experiments] further reduces the chance of partial amorphization.

The findings support the view that single QLs of Sb_2Te_3 are not robust enough to serve as crystalline spacers between actively switching GST layers. In other words, our simulations indicate

that IPCMs,^[7] i.e., superlattices that have unambiguously been shown in experiments^[14] to reconfigure into a heterostructure of rhombohedral GST and Sb₂Te₃, probably do not owe their exceptional performance to partial amorphization of thin layers. Instead, the switching mechanism probably involves crystalline–crystalline transitions that preserve the GST–Sb₂Te₃ heterostructure,^[14] e.g., models based on bilayer inversion.^[17–20]

Strictly speaking, this deduction holds only if GST layers alternate with single Sb₂Te₃ QLs in an IPCM, for a sequence of QLs might turn out to better withstand melting than a single one. The superlattice reported in the study by Simpson et al.^[7] has an overall stoichiometry of (GeTe)₂ + (Sb₂Te₃)₄. Considering the thermodynamically preferred intercalation of GeTe into Sb₂Te₃,^[14,35] it can be assumed that the superlattice^[7] comprises either alternating layers of single Ge₁Sb₂Te₄ and single Sb₂Te₃; alternating layers of (Ge₁Sb₂Te₄)₂ and (Sb₂Te₃)₂; single Ge₂Sb₂Te₅ and (Sb₂Te₃)₃; or a combination thereof. It would thus be interesting to investigate larger (and computationally more demanding) models containing a sequence of 2 or 3 Sb₂Te₃ QLs, although we believe it is likely that such models would also melt down completely in unbiased simulations, especially if they contain stacking disorder in the form of twinning.

It should be stressed that several approximations were made in our simulations. First of all, finite-size effects are significant, since our models contained 360 atoms. Furthermore, the models were heated at 1500 K to accelerate the melting process: This temperature is much higher than the experimental melting temperature of both bulk Ge₁Sb₂Te₄ and Sb₂Te₃ and can make the Sb₂Te₃ QL more prone to melting, even if the temperature is rapidly quenched after the disordering of the Ge₁Sb₂Te₄ block. Third, we used a global thermostat ensuring a uniform temperature. Other nonequilibrium effects, e.g., due to electric fields can in principle also play a role in the layered PCMs considered in this article. Therefore, further simulations going beyond these approximations would be needed to completely rule out the possibility of partial melting.

Computational Details

All simulations were performed with the CP2K suite of programs^[36] in which the Quickstep^[37] code is implemented using a mixed Gaussian and plane waves density functional theory (DFT) scheme.^[38] The Kohn–Sham states were expanded in a TZVP basis of Gaussian-type orbitals, and the plane waves for the density were cut off at 300 Ry. We used the Perdew–Burke–Ernzerhof functional based on the generalized-gradient approximation^[39] in combination with the empirical density functional theory–D2 dispersion correction^[40] and scalar-relativistic Goedecker–Teter–Hutter pseudopotentials.^[41] The Brillouin zone was sampled at the Γ point only. The molecular dynamics time step was 2 fs.

To determine the theoretical volume of the 360 atom models of Ge₁Sb₂Te₄–Sb₂Te₃ with or without twinning, the systems were relaxed in NPT simulations at 300 K and 0 Pa using Born–Oppenheimer AIMD. All other simulations were performed in the Langevin ensemble using the efficient “second-generation” Car–Parrinello-like approach to AIMD.^[42]

Our scheme to compute partial pair-correlation functions for the amorphized Ge₁Sb₂Te₄ region accounts for the finite thickness of the layer. Atoms belonging to the crystalline Sb₂Te₃ QL are ignored when building the histogram of particle–particle distances r . To restore the correct long-distance behavior of a correlation function, the histogram is normalized with respect to only that part of the surface of the sphere that lies inside

the Ge₁Sb₂Te₄ layer, i.e., $2\pi rh$ where h is the height of the sphere, the spherical cap, or the spherical segment.

To distinguish between crystalline and disordered structures on the atomic scale, we made use of the local bond-order correlation parameter q_4^{dot} .^[34] Given an atom, this quantity measures correlations in the positions of close-by atoms and, as a second step, correlates the obtained measure again with those of neighboring particles. The result is equal or close to one for a perfect crystal, whereas it assumes much lower values for atoms in liquid or amorphous environments.

Supporting Information

Supporting Information is available from the Wiley Online Library or from the author.

Acknowledgements

The authors acknowledge funding by the DFG (German Science Foundation) within the collaborative research centre SFB 917 “Nanoswitches”. The authors also acknowledge computational resources by JARA-HPC from RWTH Aachen University under projects JARA0150 and JARA0183. Open access funding enabled and organized by Projekt DEAL.

Conflict of Interest

The authors declare no conflict of interest.

Keywords

ab initio simulations, chalcogenide superlattices, molecular dynamics, phase-change materials

Received: September 21, 2020

Revised: October 8, 2020

Published online: November 9, 2020

- [1] S. Ovshinsky, *Phys. Rev. Lett.* **1968**, *21*, 1450.
- [2] M. Wuttig, N. Yamada, *Nat. Mater.* **2007**, *6*, 824.
- [3] W. Zhang, R. Mazzarello, M. Wuttig, E. Ma, *Nat. Rev. Mater.* **2019**, *4*, 150.
- [4] S. Raoux, W. Welnic, D. Ielmini, *Chem. Rev.* **2010**, *110*, 240.
- [5] J. Choe, Intel 3D XPoint Memory Die Removed from Intel Optane PCM (Phase Change Memory), <https://www.techinsights.com/blog/intel-3d-xpoint-memory-die-removed-intel-optanetm-pcm-phase-change-memory/> (accessed: October 2020).
- [6] T. C. Chong, L. P. Shi, X. Q. Wei, R. Zhao, H. K. Lee, P. Yang, A. Y. Du, *Phys. Rev. Lett.* **2008**, *100*, 136101.
- [7] R. E. Simpson, P. Fons, A. V. Kolobov, T. Fukaya, M. Krbal, T. Yagi, J. Tominaga, *Nat. Nanotechnol.* **2011**, *6*, 501.
- [8] J. Tominaga, A. V. Kolobov, P. Fons, T. Nakano, S. Murakami, *Adv. Mater. Interfaces* **2014**, *1*, 1300027.
- [9] D. Bang, H. Awano, J. Tominaga, A. V. Kolobov, P. Fons, Y. Saito, K. Makino, T. Nakano, M. Hase, Y. Takagaki, A. Giussani, R. Calarco, S. Murakami, *Sci. Rep.* **2014**, *4*, 5727.
- [10] T. Ohyanagi, M. Kitamura, M. Araidai, S. Kato, N. Takaura, K. Shiraishi, *Appl. Phys. Lett.* **2014**, *104*, 252106.
- [11] T. Egami, K. Johguchi, S. Yamazaki, K. Takeuchi, *Jpn. J. Appl. Phys.* **2014**, *53*, 04ED02.
- [12] X. Yu, J. Robertson, *Sci. Rep.* **2015**, *5*, 12612.
- [13] X. Yu, J. Robertson, *Sci. Rep.* **2016**, *6*, 37325.

- [14] J. Momand, R. Wang, J. E. Boschker, M. A. Verheijen, R. Calarco, B. J. Kooi, *Nanoscale* **2015**, *7*, 19136.
- [15] B. J. Kooi, T. M. J. De Hosson, *J. Appl. Phys.* **2002**, *92*, 3584.
- [16] A. Lotnyk, I. Hilmi, M. Behrensa, B. Rauschenbach, *Appl. Surf. Sci.* **2021**, *536*, 147959.
- [17] A. Lotnyk, U. Ross, T. Dankwort, I. Hilmi, L. Kienle, B. Rauschenbach, *Acta Mater.* **2017**, *141*, 92.
- [18] A. V. Kolobov, P. Fons, Y. Saito, J. Tominaga, *ACS Omega* **2017**, *2*, 6223.
- [19] M. Behrens, A. Lotnyk, J. W. Gerlach, I. Hilmi, T. Abel, P. Lorenz, B. Rauschenbach, *Nanoscale* **2018**, *10*, 22946.
- [20] A. Lotnyk, T. Dankwort, I. Hilmi, L. Kienle, B. Rauschenbach, *Nanoscale* **2019**, *11*, 10838.
- [21] J.-J. Wang, J. Wang, H. Du, L. Lu, P. C. Schmitz, J. Reindl, A. M. Mio, C.-L. Jia, E. Ma, R. Mazzarello, M. Wuttig, W. Zhang, *Chem. Mater.* **2018**, *30*, 4770.
- [22] J.-J. Wang, J. Wang, Y. Xu, T. Xin, Z. Song, M. Pohlmann, M. Kaminski, L. Lu, H. Du, C.-L. Jia, R. Mazzarello, M. Wuttig, W. Zhang, *Phys. Status Solidi RRL* **2019**, *13*, 1900320.
- [23] J. Feng, A. Lotnyk, H. Bryja, X. Wang, M. Xu, Q. Lin, X. Cheng, M. Xu, H. Tong, X. Miao, *ACS Appl. Mater. Interfaces* **2020**, *12*, 33397.
- [24] F. R. L. Lange, *Ph.D Thesis*, RWTH Aachen, **2016**.
- [25] M. Boniardi, J. E. Boschker, J. Momand, B. J. Kooi, A. Redaelli, R. Calarco, *Phys. Status Solidi RRL* **2019**, *13*, 1800634.
- [26] J. L. F. Da Silva, A. Walsh, H. Lee, *Phys. Rev. B* **2008**, *78*, 224111.
- [27] S. Caravati, M. Bernasconi, T. D. Kühne, M. Krack, M. Parrinello, *Appl. Phys. Lett.* **2007**, *91*, 171906.
- [28] J. Akola, R. Jones, *Phys. Rev. B* **2007**, *76*, 235201.
- [29] R. Mazzarello, S. Caravati, S. Angioletti-Uberti, M. Bernasconi, M. Parrinello, *Phys. Rev. Lett.* **2010**, *104*, 085503.
- [30] V. L. Deringer, W. Zhang, M. Lumeij, S. Maintz, M. Wuttig, R. Mazzarello, R. Dronskowski, *Angew. Chem. Int. Ed.* **2014**, *53*, 10817.
- [31] J.-Y. Raty, W. Zhang, J. Luckas, C. Chen, C. Bichara, R. Mazzarello, M. Wuttig, *Nat. Commun.* **2015**, *6*, 7467.
- [32] J. R. Errington, P. G. Debenedetti, *Nature* **2001**, *409*, 318.
- [33] I. Ronneberger, W. Zhang, H. Eshet, R. Mazzarello, *Adv. Funct. Mater.* **2015**, *25*, 6407.
- [34] P. ten Wolde, M. J. Ruiz-Montero, D. Frenkel, *Faraday Discuss.* **1996**, *104*, 93.
- [35] B. Casarin, A. Caretta, J. Momand, B. J. Kooi, M. A. Verheijen, V. Bragaglia, R. Calarco, M. Chukalina, X. Yu, J. Robertson, F. R. L. Lange, M. Wuttig, A. Redaelli, E. Varesi, F. Parmigiani, M. Malvestuto, *Sci. Rep.* **2016**, *6*, 22353.
- [36] J. Hutter, M. Iannuzzi, F. Schiffmann, J. VandeVondele, *Wiley Interdiscip. Rev.: Comput. Mol. Sci.* **2014**, *4*, 15.
- [37] J. VandeVondele, M. Krack, F. Mohamed, M. Parrinello, T. Chassaing, J. Hutter, *Comput. Phys. Commun.* **2005**, *167*, 103.
- [38] G. Lippert, J. Hutter, M. Parrinello, *Mol. Phys.* **1997**, *92*, 477.
- [39] J. P. Perdew, K. Burke, M. Ernzerhof, *Phys. Rev. Lett.* **1996**, *77*, 3865.
- [40] S. Grimme, *J. Comput. Chem.* **2006**, *27*, 1787.
- [41] S. Goedecker, M. Teter, J. Hutter, *Phys. Rev. B* **1996**, *54*, 1703.
- [42] T. D. Kühne, M. Krack, F. R. Mohamed, M. Parrinello, *Phys. Rev. Lett.* **2007**, *98*, 066401.